ViTE: Virtual Graph Trajectory Expert Router for Pedestrian Trajectory Prediction

Ruochen Li¹, Zhanxing Zhu², Tanqiu Qiao¹, Hubert P. H. Shum^{1*}

¹Department of Computer Science, Durham University, UK
²School of Electrical and Computer Science (ECS), University of Southampton, UK
{ruochen.li, hubert.shum}@durham.ac.uk

Abstract

Pedestrian trajectory prediction is critical for ensuring safety in autonomous driving, surveillance systems, and urban planning applications. While early approaches primarily focus on onehop pairwise relationships, recent studies attempt to capture high-order interactions by stacking multiple Graph Neural Network (GNN) layers. However, these approaches face a fundamental trade-off: insufficient layers may lead to underreaching problems that limit the model's receptive field, while excessive depth can result in prohibitive computational costs. We argue that an effective model should be capable of adaptively modeling both explicit one-hop interactions and implicit high-order dependencies, rather than relying solely on architectural depth. To this end, we propose ViTE (Virtual graph Trajectory Expert router), a novel framework for pedestrian trajectory prediction. ViTE consists of two key modules: a Virtual Graph that introduces dynamic virtual nodes to model long-range and high-order interactions without deep GNN stacks, and an Expert Router that adaptively selects interaction experts based on social context using a Mixture-of-Experts design. This combination enables flexible and scalable reasoning across varying interaction patterns. Experiments on three benchmarks (ETH/UCY, NBA, and SDD) demonstrate that our method consistently achieves state-of-the-art performance, validating both its effectiveness and practical efficiency.

Introduction

Human trajectory prediction aims to forecast future pedestrian paths based on observed motion histories. It plays a vital role in autonomous driving for tasks such as collision avoidance and emergency braking (Bai et al. 2015; Luo et al. 2018; Liu et al. 2021), and is also essential in video surveillance for identifying suspicious activities (Luber et al. 2010; Shi et al. 2021). This task is challenging due to the uncertainty of human behavior and the varying relevance of surrounding individuals: nearby agents may not interact, while distant ones can still be coordinated. This complexity requires models that can flexibly capture interactions across multiple scales.

Early approaches primarily focus on pairwise interactions, capturing local spatial dependencies between individuals. Representative methods like Social-LSTM (Alahi et al. 2016;

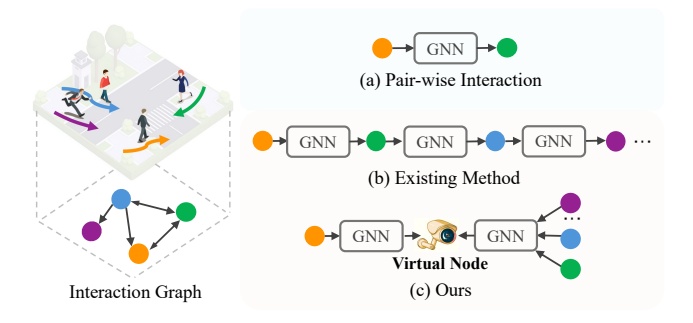


Figure 1: Comparison of interaction modeling strategies. (a) Traditional methods capture only one-hop interactions. (b) Existing methods stack multiple GNN layers to model high-order dependencies. (c) Our method introduces virtual nodes to capture high-order interactions efficiently.

Gupta et al. 2018) utilize social pooling to aggregate information from neighboring agents within a fixed window, while SS-LSTM (Xue, Huynh, and Reynolds 2018) introduces occupancy maps to encode nearby spatial configurations. With the advancement of relational modeling, graph-based methods (Huang et al. 2019; Kosaraju et al. 2019; Mohamed et al. 2020; Shi et al. 2021) have become prominent, representing pedestrians as nodes and their interactions as edges in a graph, enabling data-driven learning of pairwise relationships via Graph Neural Networks (GNNs) as shown in Figure 1 (a). To capture richer interaction dynamics, more recent efforts have focused on modeling high-order interactions—influences that are not directly observable between agent pairs but emerge through multi-hop connections within a crowd. Methods such as HighGraph (Kim et al. 2024) and PCHGCN (Chen, Sang, and Zhao 2025) address this by stacking multiple GNN layers (Figure 1 (b)), allowing information to propagate across longer distances and indirectly connected agents. These models have shown improvements in capturing group behavior patterns and non-local dependencies.

Despite their effectiveness, high-order interaction modeling via deep GNNs introduces two key challenges. The first is depth-related inefficiency. Stacking too few GNN layers results in under-reaching, where the receptive field is insufficient to cover relevant agents beyond local neighborhoods, leading to incomplete interaction modeling (Lu

^{*}Corresponding author Copyright © 2026, Association for the Advancement of Artificial Intelligence (www.aaai.org). All rights reserved.

et al. 2024). Conversely, increasing depth can cause oversmoothing (Rusch, Bronstein, and Mishra 2023), where repeated message passing dilutes node-specific features, making individual agent representations less discriminative. This trade-off poses a fundamental bottleneck for graph-based trajectory models that rely solely on depth to model relational complexity. Another major limitation is the lack of contextual adaptability. In real-world crowds, the influence of other pedestrians varies across scenes and situations: in some cases, immediate neighbors dominate decision-making, while in others, long-range or indirect interactions play a critical role. However, most existing methods apply a fixed, shared relational structure or aggregation scheme to all agents, ignoring this diversity. As a result, they fail to dynamically adjust the reasoning process according to individual agents' social context and interaction scale.

To address these limitations, we propose ViTE (Virtual graph Trajectory Expert router), a novel framework for pedestrian trajectory prediction. It comprises two key components. First, the Virtual Graph, introduces dynamically assigned virtual nodes that act as relational mediators between pedestrians (Figure 1 (c)). These nodes serve as intermediate hubs for message exchange, enabling the model to capture longrange dependencies and high-order interactions without deep GNN stacks. This compact and learnable structure not only mitigates under-reaching but also improves efficiency and expressiveness in modeling long-range relations. Second, the Expert Router adopts a Mixture-of-Experts (MoE) design to enable context-aware interaction reasoning. We introduce multiple interaction experts, each specialized in a particular interaction scale (e.g., one-hop or high-order), are coordinated by a gating network that dynamically routes each agent's representation to the most relevant experts. This adaptive mechanism allows ViTE to flexibly integrate diverse relational patterns based on social context. Together, these two modules form a cohesive and scalable system that overcomes depth limitations and enables fine-grained social reasoning for trajectory prediction. Our main contributions are:

- We propose ViTE, a novel framework for pedestrian trajectory prediction that enables efficient and adaptive highorder interaction modeling.
- We design a Virtual Graph module that introduces dynamic virtual nodes as relational hubs to capture indirect social dependencies.
- We develop an Expert Router based on a Mixture-of-Experts mechanism to perform context-aware reasoning across multiple interaction scales.

Code: https://github.com/Carrotsniper/ViTE

Related Work

Interaction Modeling for Trajectory Prediction

Early work on pedestrian trajectory prediction focused on pairwise interactions to capture the influence of nearby agents. Social-LSTM (Alahi et al. 2016; Gupta et al. 2018) introduced a pooling mechanism to aggregate neighboring hidden states, while SS-LSTM (Xue, Huynh, and Reynolds 2018) encoded spatial layouts via occupancy maps to enhance local

interaction modeling. However, these methods struggle with complex multi-agent dynamics due to their limited relational structure. To address this, graph-based approaches (Bae and Jeon 2021; Qiao et al. 2022; Bae and Jeon 2023; Qiao et al. 2024) have been proposed, representing pedestrians as nodes and their interactions as edges in a graph. ST-GAT (Huang et al. 2019) employs graph attention (Qiao et al. 2025; Shao et al. 2025b,a) to adaptively weigh neighboring influences, Social-STGCNN (Mohamed et al. 2020) combines spatial and temporal convolutions, Social-BiGAT (Kosaraju et al. 2019) models bidirectional influence flows, and SGCN (Shi et al. 2021) applies sparse GCNs to capture spatial-temporal dependencies. These methods advance beyond pairwise designs by leveraging GNNs to jointly model spatial and temporal dependencies. To capture high-order interactions, which refer to indirect influences mediated through intermediate agents, recent works such as HighGraph (Kim et al. 2024) and PCHGCN (Chen, Sang, and Zhao 2025) stack multiple GNN layers to enable multi-hop message passing. While effective for modeling non-local dependencies, this strategy faces a trade-off: shallow networks suffer from under-reaching (Lu et al. 2024; Li et al. 2025b), while deeper ones risk oversmoothing, degrading representation quality (Rusch, Bronstein, and Mishra 2023). To this end, we introduce adaptive virtual nodes that serve as global relational hubs, effectively capturing high-order interactions by mediating indirect dependencies without relying on deep GNNs.

Mixture of Expert

Mixture of Experts (MoE) is a modular neural architecture that partitions the input space and routes each input to a subset of specialized experts, selected dynamically by a gating network (Yuksel, Wilson, and Gader 2012; Jiang et al. 2024; Mu and Lin 2025). Unlike traditional ensembles, MoE activates only a few experts per input, enabling high model capacity with reduced computational cost. This design has shown success in NLP (Jacobs et al. 1991; Shazeer et al. 2017), vision (Wang et al. 2020; Riquelme et al. 2021), and multi-modal learning (Mustafa et al. 2022). In graph learning, MoE has been applied to aggregate across neighborhoods (Abu-El-Haija et al. 2020), correct bias (Hu et al. 2022), and enhance molecular prediction (Kim et al. 2023). Recent works explore top-k input routing (Zhou et al. 2022) and multi-hop fusion (Wang et al. 2023), but often rely on fixed routing or task-specific designs, limiting adaptability. In this work, we propose a MoE-based expert router for trajectory prediction, which enables context-aware routing over one-hop and highorder graph interactions. By dynamically selecting the most relevant expert for each node, our model effectively adapts to diverse interactions in pedestrian crowds.

Methodology

Problem Formulation

Pedestrian trajectory prediction forecasts future positions from past movements. Mathematically, given a scene with N pedestrians observed over T_{obs} time steps, the trajectory of pedestrian i is denoted as $X_i = (x_t^i, y_t^i) \mid t \in [-T_{obs} + 1, \dots, 0]$ for the observed past, and

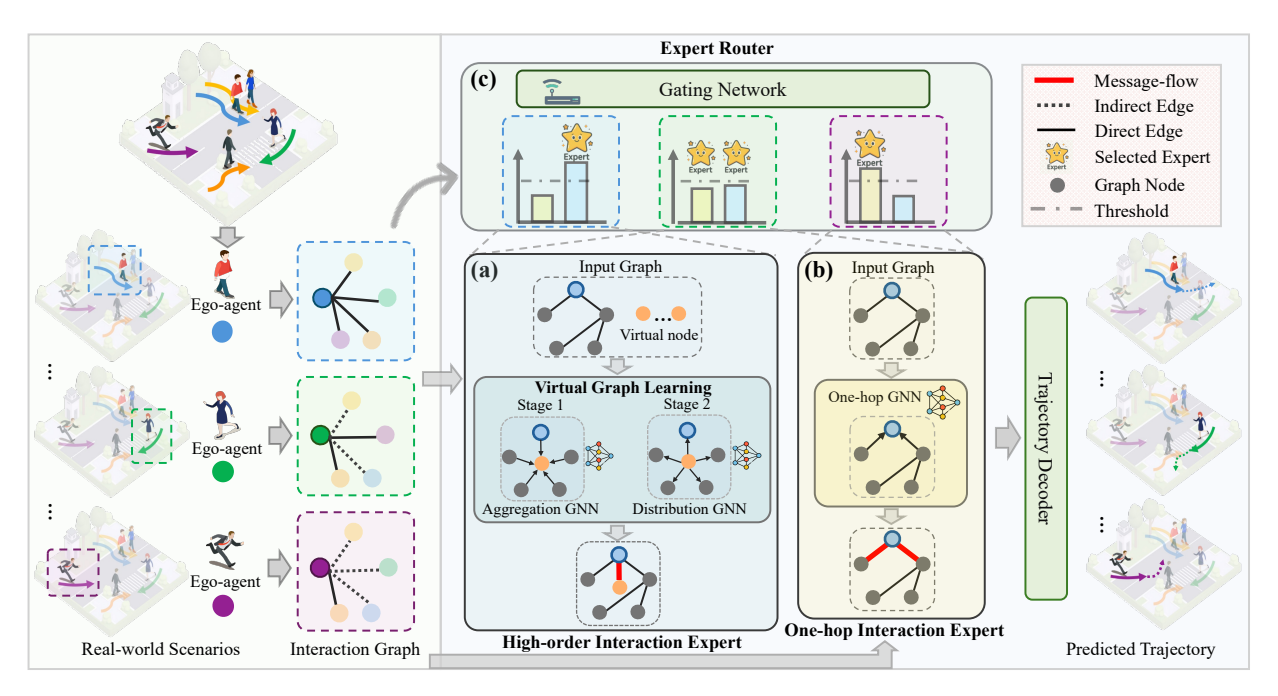


Figure 2: Overview of ViTE. Given pedestrian trajectories, we first construct interaction graphs. In (a), the high-order interaction expert captures indirect, long-range dependencies via Virtual Graph Learning, while (b) illustrates the one-hop expert modeling direct interactions. These expert outputs are then dynamically fused by a MoE-based Expert Router, as depicted in (c), enabling context-aware routing of graph information. Finally, an MLP-based decoder outputs future trajectories for each pedestrian.

 $Y_i = (x_t^i, y_t^i) \mid t \in [1, \dots, T_{pred}]$ for the future ground-truth. Stacking all pedestrians yields the tensors $\mathbf{X} \in \mathbb{R}^{N \times T_{obs} \times 2}$ and $\mathbf{Y} \in \mathbb{R}^{N \times T_{pred} \times 2}$, representing the observed and future trajectories respectively, with each position in 2D coordinates. The goal is to minimize the error between the predicted trajectories $\hat{\mathbf{Y}}$ and ground-truth future trajectories \mathbf{Y} .

Feature Initialization

For each pedestrian i, we construct the input representation from two complementary feature types: absolute spatial coordinates $\mathbf{p}_i = (x,y)$ and temporal displacement vectors $\mathbf{r}_i = (r_x, r_y)$, where $\mathbf{r}_i^{(t)} = \mathbf{p}_i^{(t)} - \mathbf{p}_i^{(t-1)}$ captures the motion dynamics. The final input feature is obtained through concatenation: $\mathbf{X}_i^{\text{in}} = [\mathbf{p}_i; \mathbf{r}_i] \in \mathbb{R}^{T_{obs} \times 4}$. We represent pedestrian interactions using a spatial interaction graph $\mathcal{G} = (\mathcal{V}, \mathcal{E})$, where each node $n_i \in \mathcal{V}$ corresponds to pedestrian i, and each edge $e_{ij} \in \mathcal{E}$ models one-hop relationships. Node features are initialized as $\mathbf{n}_i^{(0)} = \mathcal{F}_{node}(\mathbf{X}_i^{\text{in}})$, where $\mathcal{F}_{node}(\cdot)$ denotes a Multi-Layer Perceptron (MLP). To capture social dependencies, we dynamically determine the graph connectivity via a k-nearest neighbor strategy based on feature similarity. For each connected pair (i,j), we compute the initial embedding feature using a relational transformer (RT) layer (Diao and Loynd 2023; Lee et al. 2024) equipped with sparse attention to ensure computational efficiency, denoted as $\mathbf{n}_{i,pair}^0 = RT(\mathbf{n}_i^{(0)}, M)$, where M is connection mask.

High-order Interaction Modeling via Virtual Graph

Capturing long-range dependencies is essential in trajectory prediction, as agents often influence one another beyond their immediate neighbors through high-order interactions. However, traditional GNNs based on first-order aggregation inherently suffer from *under-reaching*—the inability to propagate information across distant nodes within shallow architectures (Qian et al. 2024). Although stacking GNN layers helps capture high-order interactions (Kim et al. 2024; Chen, Sang, and Zhao 2025), it significantly increases computational cost.

To quantify this limitation, we calculate the *effective resistance* as a structural indicator of communication efficiency in graphs. Formally, the effective resistance between two nodes i and j is defined as:

$$R_{ij} = (e_i - e_j)^T \mathcal{L}^+(e_i - e_j),$$
 (1)

where \mathcal{L}^+ is the Moore–Penrose pseudoinverse of the graph Laplacian, and e_i, e_j are standard basis vectors. Lower R_{ij} indicates more efficient message propagation (Lu et al. 2024). For example, in the chain-structured graph shown in Figure 3 (left), node a requires four hops to reach node e, resulting in a high resistance of $R_{ae}=4.0$, which hinders the efficiency of long-range communication.

To address this issue, we propose the **Virtual Graph**, which introduces a small set of virtual nodes as mediators to facilitate high-order long-range communication. As shown in Figure 3 (right), adding a virtual node dramatically reduces the resistance between distant nodes (e.g., $R_{ae} = 1.2$), enabling more efficient global information flow.

Specifically, we construct a high-order interaction graph $\mathcal{G}_{high} = (\mathcal{N} \cup \mathcal{V}_{virtual}, \mathcal{E}_{high})$, where \mathcal{N} denotes the set of real

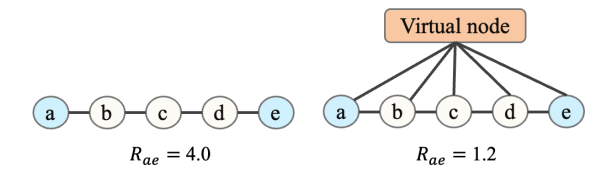


Figure 3: Comparison of effective resistance (R_{ae}) between a standard chain graph (left, $R_{ae}=4.0$) and a virtual-node-enhanced graph structure (right, $R_{ae}=1.2$). Lower effective resistance indicates more efficient message propagation and improved global connectivity.

pedestrian nodes, and $\mathcal{V}_{\text{virtual}} = \{v_1, v_2, \dots, v_V\}$ is a set of virtual nodes acting as communication hubs. These virtual nodes are instantiated per training batch and initialized with diverse embeddings sampled from a learnable distribution:

$$\mathbf{v}_k^{(0)} \sim \mathcal{D}_{\text{vn}}, \quad k = 1, \dots, V,$$
 (2)

where \mathcal{D}_{vn} is designed to promote representational diversity. To explicitly capture high-order dependencies, we propose a structured two-stage message passing scheme.

Stage 1 (Real-to-Virtual Message Aggregation). Each real node $n_i \in \mathcal{N}$ sends its node embedding to all virtual nodes, enabling them to aggregate diverse contexts into high-level representations. The embedding of each virtual node v_k is updated as:

$$\mathbf{v}_{k}^{(1)} = \text{GNN}_{r \to v} \left(\mathbf{v}_{k}^{(0)}, \text{AGG}_{r \to v} \left(\left\{ \mathbf{n}_{i}^{(0)} \mid n_{i} \in \mathcal{N} \right\} \right) \right),$$
(3

where $AGG_{r \to v}$ is a permutation-invariant aggregator (e.g., mean or attention), and $GNN_{r \to v}$ is a standard GNN module such as a Graph Attention Network (Veličković et al. 2018).

Stage 2 (Virtual-to-Real Message Distribution). Each updated virtual node v_k broadcasts its high-level contexts to all pedestrian nodes, enabling them to integrate indirect high-order interactions into their representations. The embedding of each pedestrian node n_i is updated as:

$$\mathbf{n}_{i}^{(1)} = \text{GNN}_{\mathbf{v} \to \mathbf{r}} \left(\mathbf{n}_{i}^{(0)}, \text{AGG}_{\mathbf{v} \to \mathbf{r}} \left(\left\{ \mathbf{v}_{k}^{(1)} \mid v_{k} \in \mathcal{V} \right\} \right) \right), \tag{4}$$

where $AGG_{v \to r}$ is a permutation-invariant aggregator, and $GNN_{v \to r}$ is a standard GNN module for fusing virtual node information. The final output is then normalized and activated as: $\mathbf{n}_{i, \text{high}}^{(\text{out})} = \text{GELU}\left(\text{LayerNorm}\left(\mathbf{n}_i^{(1)}\right)\right)$.

In summary, our virtual graph interaction module integrates both localized and global context by combining one-hop and high-order message passing mechanisms. The one-hop graph captures fine-grained local interactions among neighboring agents, while the virtual-node-enhanced graph enables efficient modeling of high-order dependencies. Together, these complementary designs equip the model with a more expressive and scalable interaction representation.

One-hop Interaction Modeling

To capture one-hop interactions among pedestrians, we define a first-order directed interaction graph $\mathcal{G}_{\text{one-hop}}$ =

 $(\mathcal{N}, \mathcal{E}_{\text{one-hop}})$, where edges $\mathcal{E}_{\text{one-hop}}$ encode spatial relationships between neighboring agents based on their similarities (Lee et al. 2024). This graph supports message passing operations in GNNs, enabling the modeling of one-hop dependencies among directly connected nodes (Li, Katsigiannis, and Shum 2022; Li et al. 2025a).

The expert leverages both node and edge features to update each node embedding. Specifically, each node n_i aggregates information from its neighbors as follows:

$$\mathbf{m}_{ij} = \phi_m \left(\mathbf{n}_i^{(0)}, \mathbf{n}_j^{(0)}, \mathbf{e}_{ij}^{(0)} \right), \tag{5}$$

$$\mathbf{m}_{i} = AGG_{\text{one-hop}}(\{\mathbf{m}_{ij} \mid j \in \mathcal{N}_{\text{one-hop}}(i)\}),$$
 (6)

$$\mathbf{n}_{i,\text{one-hop}}^{(\text{out})} = \phi_u \left(\mathbf{n}_i^{(0)}, \mathbf{m}_i \right), \tag{7}$$

where $\phi_m(\cdot)$ denotes the message function that integrates source node, target node, and edge features; $AGG_{one-hop}(\cdot)$ is a permutation-invariant aggregation function; and $\phi_u(\cdot)$ is the update function, typically an MLP layer. This design allows the model to leverage both one-hop structural information and relation features for direct interaction modeling.

Expert Router

While one-hop and high-order graph structures capture complementary interaction patterns, existing methods typically adopt a fixed graph design, limiting adaptability to varying scene complexities. Such rigidity can result in under-reaching in complex scenarios or redundant computation in simpler ones. To address this limitation, we propose an adaptive **Expert Router** based on the MoE paradigm, which learns a context-aware routing policy to dynamically allocate interaction modeling capacity. Specifically, we treat $\mathcal{G}_{\text{one-hop}}$ and $\mathcal{G}_{\text{high}}$ as two specialized experts responsible for modeling direct and high-order interactions, respectively. By allowing each node to selectively attend to the most relevant expert based on its feature representations.

For each node feature $\mathbf{n}_i^{(0)}$, the gating network computes a soft routing distribution (Hu et al. 2025) over the two experts:

$$\mathbf{g}_i = \text{Softmax}(\phi(\mathbf{n}_i^{(0)})), \tag{8}$$

$$\phi(\mathbf{n}_i^{(0)}) = \mathbf{W}_g \mathbf{n}_i^{(0)} + \epsilon \cdot \text{Softplus}(\mathbf{W}_n \mathbf{n}_i^{(0)}), \qquad (9)$$

where $\phi(\mathbf{n}_i^{(0)}) \in \mathbb{R}^2$ are the logits over two experts, and $\epsilon \sim \mathcal{N}(\mathbf{0}, \mathbf{I})$ adds Gaussian noise for regularization. \mathbf{W}_g and \mathbf{W}_n are learnable projection matrices.

To enable adaptive complexity control and improve efficiency, we adopt a threshold-based Top-P mechanism that dynamically selects active experts (Huang et al. 2024; Hu et al. 2025). Unlike traditional MoE methods (Wang et al. 2023) that always fuse all experts, our approach activates experts based on confidence, enabling lightweight local processing for simple cases and triggering global reasoning in complex interaction scenarios.

Let $\tilde{g}_i = \text{Sort}(g_i, \text{descending})$ be the sorted expert probabilities. The active expert set S_i is defined as the minimal set

| ETH/UCY Dataset | | | | | | | | | | |
|-----------------|-----------|-------------------|-------------------|-------------------|---------------------------|-------------------|---------------------------|---------------------------|---------------------------|---|
| Subset | GroupNet | MemoNet | MID | NPSN | EqMotion | EigenTraj | LED | SingularTraj | MART | PCHGCN Ours |
| ETH | 0.46/0.73 | 0.40/0.61 | 0.39/0.66 | 0.36/0.59 | 0.40/0.61 | 0.36/0.53 | 0.39/0.58 | 0.35/0.42 | 0.35 / <u>0.47</u> | 0.42/0.65 0.35 /0.49 |
| HOTEL | 0.15/0.25 | 0.11/0.17 | 0.13/0.22 | 0.16/0.25 | 0.12/0.18 | 0.12/0.19 | 0.11/0.17 | 0.13/0.19 | 0.14/0.22 | 0.17/0.28 0.11/0.17 |
| UNIV | 0.26/0.49 | 0.24/0.43 | 0.22/0.45 | 0.23/0.39 | 0.23/0.43 | 0.24/0.43 | 0.26/0.43 | 0.25/0.44 | 0.25/0.45 | 0.21/0.38 0.23/0.42 |
| ZARA1 | 0.21/0.39 | 0.18/0.32 | 0.17 /0.30 | 0.18/0.32 | 0.18/0.32 | 0.19/0.33 | <u>0.18</u> / 0.26 | 0.19/0.32 | 0.17 / <u>0.29</u> | 0.17 /0.31 <u>0.18</u> /0.30 |
| ZARA2 | 0.17/0.33 | <u>0.14</u> /0.24 | 0.13 /0.27 | <u>0.14</u> /0.25 | 0.13 / <u>0.23</u> | <u>0.14</u> /0.24 | 0.13/0.22 | 0.15/0.25 | 0.13/0.22 | 0.13 / <u>0.23</u> 0.13 / 0.22 |
| AVG | 0.25/0.44 | 0.21/0.35 | 0.21/0.38 | 0.21/0.36 | 0.21/0.35 | 0.21/0.34 | 0.21/0.33 | <u>0.21</u> / 0.32 | 0.21/0.33 | 0.22/0.37 0.20/0.32 |

Table 1: Performance comparison on the ETH/UCY dataset. Metrics are $\min ADE_{20}/\min FDE_{20}$. **Bold** and <u>underline</u> indicate the best and second-best results.

| | NBA Dataset | | | | | | | | |
|------|-------------|-----------|-----------|-----------|-----------|-------------|-----------|--------------|---|
| Time | STAR | GroupNet | MemoNet | MID | NPSN | DynGroupNet | LED | SingularTraj | MART Ours |
| 1.0s | 0.43/0.66 | 0.26/0.34 | 0.38/0.56 | 0.28/0.37 | 0.35/0.58 | 0.19/0.28 | 0.18/0.27 | 0.28/0.44 | <u>0.18/0.26</u> 0.17/0.25 |
| 2.0s | 0.75/1.24 | 0.49/0.70 | 0.71/1.14 | 0.51/0.72 | 0.68/1.23 | 0.40/0.61 | 0.37/0.56 | 0.61/1.00 | 0.35/0.50 0.35/0.50 |
| 3.0s | 1.03/1.51 | 0.73/1.02 | 1.00/1.57 | 0.71/0.98 | 1.01/1.76 | 0.65/0.90 | 0.58/0.84 | 0.96/1.47 | <u>0.54/0.71</u> 0.53/0.70 |
| 4.0s | 1.13/2.01 | 0.96/1.30 | 1.25/1.47 | 0.96/1.27 | 1.31/1.79 | 0.89/1.13 | 0.81/1.10 | 1.31/1.98 | <u>0.73/0.90</u> 0.72 / <u>0.91</u> |

Table 2: Performance comparison on the NBA dataset. Metrics are $\min ADE_{20}/\min FDE_{20}$. **Bold** and <u>underline</u> indicate the best and second-best results.

whose cumulative probability exceeds a threshold p:

$$S_i = \left\{ k : \sum_{j=1}^k \tilde{g}_{i,j} \le p \right\} \cup \left\{ \arg\min_k \left\{ \sum_{j=1}^k \tilde{g}_{i,j} > p \right\} \right\},$$
(10)

where $p \in (0,1)$ controls the sparsity level (e.g., p = 0.7). The selected expert weights are then renormalized as:

$$\hat{g}_{i,k} = \begin{cases} \frac{g_{i,k}}{\sum_{j \in \mathcal{S}_i} g_{i,j}} & \text{if } k \in \mathcal{S}_i, \\ 0 & \text{otherwise.} \end{cases}$$
 (11)

Given the selected expert set S_i and renormalized weights $\hat{g}_{i,k}$ from Eq. 11, the final node representation is computed as a weighted sum:

$$\mathbf{n}_{i,router}^{(\text{out})} = \hat{g}_{i,1} \cdot \mathbf{n}_{i,\text{one-hop}}^{(\text{out})} + \hat{g}_{i,2} \cdot \mathbf{n}_{i,\text{high}}^{(\text{out})}. \tag{12}$$

By leveraging soft gating and selective expert activation, the proposed **Expert Router** enables context-aware routing of one-hop and high-order interactions, allowing the model to dynamically adjust its reasoning complexity based on pedestrian behavior patterns.

To prevent routing collapse and promote expert diversity, we introduce an importance-based auxiliary loss (Hu et al. 2025):

$$\mathcal{L}_{imp} = \frac{1}{N} \sum_{i=1}^{N} \frac{Std(\mathbf{g}_i)}{Mean(\mathbf{g}_i) + \epsilon},$$
(13)

which encourages balanced expert utilization across nodes and improves the robustness of the routing mechanism.

Trajectory Decoding

For trajectory prediction, we concatenate three feature types $[\mathbf{n}_i^{(0)}; \mathbf{n}_{i,pair}^{(0)}; \mathbf{n}_{i,router}^{(\text{out})}]$ and feed them into K parallel MLP-

based prediction heads to generate diverse trajectories following (Xu et al. 2023; Lee et al. 2024). Given K predicted trajectories $\hat{\mathbf{Y}}_i^{(k)}$ from K prediction heads for pedestrian i, we compute the prediction loss by selecting the best trajectory in terms of minimum ℓ_2 distance to the ground truth:

$$\mathcal{L}_{\text{pred}} = \frac{1}{NT_{pred}} \sum_{i=1}^{N} \sum_{t=1}^{T_{pred}} \min_{k} ||\mathbf{p}_{i}^{(t)} - \hat{\mathbf{p}}_{i}^{(t,k)}||_{2}, \quad (14)$$

where $\mathbf{p}_i^{(t)} = (x_t^i, y_t^i)$ is the ground-truth position of pedestrian i at time t, and $\hat{\mathbf{p}}_i^{(t,k)}$ is the corresponding prediction from the k-th head. The total loss incorporates MoE regularization: $\mathcal{L} = \mathcal{L}_{\text{pred}} + \lambda \mathcal{L}_{\text{imp}}$.

Experiments

Experimental Setup

Datasets. We evaluate our model on three widely-used trajectory prediction benchmarks: ETH/UCY (Pellegrini et al. 2009; Lerner, Chrysanthou, and Lischinski 2007), Stanford Drone Dataset (SDD) (Robicquet et al. 2016), and NBA SportVU (Mao et al. 2023). The ETH/UCY dataset comprises five subsets (ETH, HOTEL, UNIV, ZARA1, and ZARA2), capturing pedestrian movements across diverse social scenarios. SDD is a large-scale dataset collected from a university campus. For both ETH/UCY and SDD, we follow the standard setting in (Lee et al. 2024; Xu et al. 2022b), using 3.2 seconds (8 frames) of observed trajectories to predict the next 4.8 seconds (12 frames). For ETH/UCY, we adopt a leaveone-out training protocol, training on four subsets and testing on the remaining one. The NBA SportVU dataset provides trajectories of 10 players and the ball in real basketball games. We follow (Xu et al. 2022a; Mao et al. 2023; Lee et al. 2024)

| SDD Dataset | | | | | | | | | |
|-------------------|------------|------------|------------|------------|-------------|------------|------------|------------|--------------------|
| Time PECNet | GroupNet | MemoNet | MID | NPSN | DynGroupNet | EigenTraj | LED | MART | Ours |
| 4.8s 9.96/15.88 | 9.31/16.11 | 8.56/12.66 | 9.73/15.32 | 8.56/11.85 | 8.42/13.58 | 8.05/13.25 | 8.48/11.66 | 7.43/11.82 | 7.42 /11.90 |

Table 3: Performance comparison on the SDD dataset. Metrics are $\min ADE_{20}/\min FDE_{20}$. **Bold** and <u>underline</u> indicate the best and second-best results.

that use 2.0 seconds (10 frames) of past motion to predict the next 4.0 seconds (20 frames).

Evaluation Metrics. To evaluate the performance, we adopt two metrics: $\min ADE_k$ and $\min FDE_k$, following the evaluation protocol in (Gupta et al. 2018; Lee et al. 2024). The Average Displacement Error (ADE) measures the mean Euclidean distance between the predicted and ground-truth trajectories over all time steps, while the Final Displacement Error (FDE) focuses on the distance between the predicted and actual final positions. Given k sampled predictions for each agent, we report the minimum ADE and FDE among them, denoted as $\min ADE_k$ and $\min FDE_k$.

Comparison with State-of-the-Art Methods

The results on the ETH/UCY dataset are presented in Table 1, our method achieves the best overall performance, with the lowest average ADE/FDE of 0.20/0.32 across all five subsets. Compared to PCHGCN, a high-order graphbased method, our approach reduces ADE by 9.1% and FDE by 13.5%. Moreover, our method consistently ranks among the top performers on each individual subset, demonstrating strong generalization across diverse crowd scenarios. For NBA datasets shown in Table 2, our model ranks first at 1.0s, 2.0s, and 3.0s, and achieves the lowest ADE and secondbest FDE at 4.0s, highlighting its robustness in modeling long-term multi-agent interactions in dynamic sports environments. Table 3 presents the results on the SDD dataset. Our method achieves the best ADE and a competitive FDE compared to existing approaches, confirming its effectiveness in forecasting pedestrian trajectories in real-world scenes.

Ablation Study and Analysis

Effect of Expert. We conduct ablation studies to assess the impact of different configurations of Expert Router (Table 4). Removing both experts results in a clear performance drop, confirming the necessity of incorporating expert mechanisms into the model. When comparing single-expert settings, the one-hop expert yields better results than the high-order counterpart, indicating that certain interaction structures are more informative for prediction. Most notably, our adaptive MoE outperforms both individual experts and the fixed mixed configuration, demonstrating that dynamic, input-dependent expert selection offers clear advantages over static alternatives. These findings validate the effectiveness of context-aware expert routing in modeling diverse trajectory patterns.

Effect of Virtual Nodes. To assess the effectiveness of the Virtual Graph, we compare our model with conventional multi-layer GCNs. As shown in Table 6, our approach achieves the best performance with the fewest parameters

| Expert Configuration | ETH/UCY Dataset | | | | |
|-----------------------------|--------------------------|--------------------------|--|--|--|
| | $\min \mathrm{ADE}_{20}$ | $\min \mathrm{FDE}_{20}$ | | | |
| One-hop Expert Only | 0.22 | 0.34 | | | |
| High-order Expert Only | 0.23 | 0.36 | | | |
| Mixed Expert | 0.25 | 0.36 | | | |
| No Expert | 0.25 | 0.38 | | | |
| Ours | 0.20 | 0.32 | | | |

Table 4: Ablation study of expert selection evaluated by $\min ADE_{20}/\min FDE_{20}$ on ETH/UCY dataset. **Bold** and underline indicate the best and second-best results.

| Method | #Param. | MACs |
|----------|--------------|---------------|
| PECNet | 2.1M | 259.2M |
| STAR | 1.0M | 12.0G |
| MemoNet | 10.7M | 6.0G |
| GroupNet | 2.2M | 411.5M |
| MID | 9.0M | 40.3G |
| EqMotion | 3.0M | 147.1M |
| LED | 10.9M | 15.0G |
| MART | <u>1.5</u> M | <u>43.3</u> M |
| Ours | 1.0M | 23.1 M |

Table 5: Model complexity comparison. **Bold** and <u>underline</u> indicate the best and second-best results.

(1.00×), outperforming both 2-layer and 4-layer GCNs. Notably, simply increasing GCN depth does not yield better results—the 4-layer model even slightly underperforms the 2-layer variant, despite having more parameters. This suggests that stacking layers is neither efficient nor sufficient for capturing high-order interactions. In contrast, our use of virtual nodes offers a more effective and parameter-efficient solution for modeling such interactions.

Efficiency Comparisons. Table 5 compares model complexity in terms of parameters and Multiply–Accumulate Operations (MACs). Following the evaluation protocol of (Lee et al. 2024), we compute MACs using scenes with 10 agents from the ETH/UCY dataset. Our method achieves the lowest computational complexity (23.1M MACs) and the smallest parameter count (1.0M) among all baselines. These results highlight the efficiency of our model and its suitability for real-world deployment.

Qualitative Results

Visualization of Predicted Trajectory. Figure 4 shows qualitative comparisons on the ETH/UCY dataset among EigenTraj, MART, and our model. Our predictions (green)

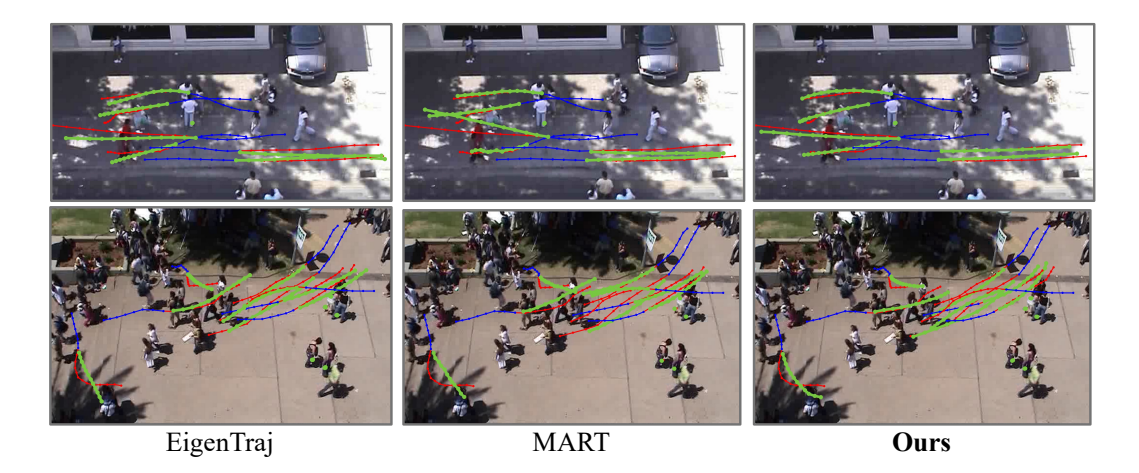


Figure 4: Qualitative results on ETH/UCY datasets. Historical trajectories are in blue, ground-truth trajectories are in red, and predicted trajectories are in green.

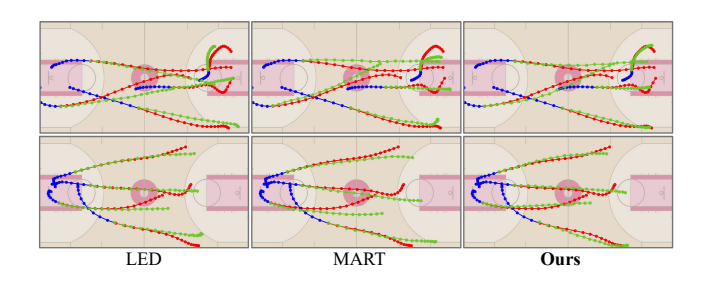


Figure 5: Qualitative results on NBA datasets. Historical trajectories are in blue, ground-truth trajectories are in red, and predicted trajectories are in green.

| Variant | ETH/UCY Dataset | | | | | | |
|---------------|--------------------------|--------------------------|--------------|--|--|--|--|
| | $\min \mathrm{ADE}_{20}$ | $\min \mathrm{FDE}_{20}$ | Param. Ratio | | | | |
| GCN (2-layer) | 0.22 | 0.36 | 0.97x | | | | |
| GCN (4-layer) | 0.23 | 0.36 | 1.11x | | | | |
| Ours | 0.20 | 0.32 | 1.00x | | | | |

Table 6: Ablation study on virtual graph effectiveness evaluated by $\min ADE_{20}/\min FDE_{20}$ on ETH/UCY dataset. **Bold** and underline indicate the best and second-best results.

align more closely with ground-truth trajectories (red), capturing pedestrians' subtle movements and social interactions more accurately. Figure 5 presents trajectory predictions on the NBA dataset comparing LED, MART, and our approach. Our method consistently generates smoother and more precise trajectories, effectively capturing complex dynamics and long-term interactions among multiple agents. These visual results further confirm our model's superior predictive capability across diverse scenarios.

Expert Weight Analysis. Figure 6 illustrates the learned expert weights for different trajectory scenarios. The results indicate that the one-hop expert generally receives higher

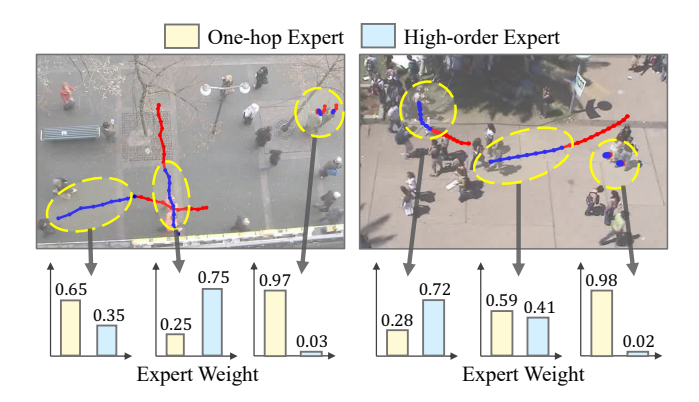


Figure 6: Visualization of learned expert weights across different scenarios. The model dynamically adjusts one-hop and high-order expert contributions by interaction complexity.

weights in simpler interactions. Conversely, the high-order expert dominates in more complex, globally interactive scenarios. This adaptive expert weighting confirms the effectiveness of our model in dynamically balancing the usage of one-hop expert and high-order expert.

Conclusion

We propose ViTE, a novel trajectory prediction framework combining Virtual Graph for high-order interactions and Expert Router for adaptive expert routing. This design balances multi-scale reasoning and computational efficiency. Experiments on ETH/UCY, NBA, and SDD confirm state-of-the-art performance. Future work will incorporate contextual image information to further enhance scene understanding. Integrating visual semantics such as obstacles, road structure, or group behavior cues could provide stronger priors for trajectory prediction. We also aim to explore more flexible expert architectures that dynamically adjust their granularity or number based on scene complexity.

Acknowledgment

This project is supported in part by the EPSRC NortHFutures project (ref: EP/X031012/1).

References

- Abu-El-Haija, S.; Kapoor, A.; Perozzi, B.; and Lee, J. 2020. N-gcn: Multi-scale graph convolution for semi-supervised node classification. In *UAI*, 841–851.
- Alahi, A.; Goel, K.; Ramanathan, V.; Robicquet, A.; Fei-Fei, L.; and Savarese, S. 2016. Social lstm: Human trajectory prediction in crowded spaces. In *CVPR*, 961–971.
- Bae, I.; and Jeon, H.-G. 2021. Disentangled multi-relational graph convolutional network for pedestrian trajectory prediction. In *AAAI*, volume 35, 911–919.
- Bae, I.; and Jeon, H.-G. 2023. A set of control points conditioned pedestrian trajectory prediction. In *AAAI*, volume 37, 6155–6165.
- Bai, H.; Cai, S.; Ye, N.; Hsu, D.; and Lee, W. S. 2015. Intention-aware online POMDP planning for autonomous driving in a crowd. In *ICRA*, 454–460.
- Chen, W.; Sang, H.; and Zhao, Z. 2025. PCHGCN: Physically Constrained Higher-Order Graph Convolutional Network for Pedestrian Trajectory Prediction. *IEEE Internet of Things Journal*, 12(13): 25033–25045.
- Diao, C.; and Loynd, R. 2023. Relational Attention: Generalizing Transformers for Graph-Structured Tasks. In *ICLR*.
- Gupta, A.; Johnson, J.; Fei-Fei, L.; Savarese, S.; and Alahi, A. 2018. Social gan: Socially acceptable trajectories with generative adversarial networks. In *CVPR*, 2255–2264.
- Hu, F.; Wang, L.; Wu, S.; Wang, L.; and Tan, T. 2022. Graph classification by mixture of diverse experts. *IJCAI*.
- Hu, Y.; Zhang, G.; Liu, P.; Lan, D.; Li, N.; Cheng, D.; Dai, T.; Xia, S.-T.; and Pan, S. 2025. TimeFilter: Patch-Specific Spatial-Temporal Graph Filtration for Time Series Forecasting. In *ICML*.
- Huang, Q.; An, Z.; Zhuang, N.; Tao, M.; Zhang, C.; Jin, Y.; Xu, K.; Xu, K.; Chen, L.; Huang, S.; and Feng, Y. 2024. Harder Task Needs More Experts: Dynamic Routing in MoE Models. In *ACL*, 12883–12895.
- Huang, Y.; Bi, H.; Li, Z.; Mao, T.; and Wang, Z. 2019. Stgat: Modeling spatial-temporal interactions for human trajectory prediction. In *ICCV*, 6272–6281.
- Jacobs, R. A.; Jordan, M. I.; Nowlan, S. J.; and Hinton, G. E. 1991. Adaptive mixtures of local experts. *Neural Computation*, 3(1): 79–87.
- Jiang, W.; Han, J.; Liu, H.; Tao, T.; Tan, N.; and Xiong, H. 2024. Interpretable cascading mixture-of-experts for urban traffic congestion prediction. In *SIGKDD*, 5206–5217.
- Kim, S.; Chi, H.-g.; Lim, H.; Ramani, K.; Kim, J.; and Kim, S. 2024. Higher-order Relational Reasoning for Pedestrian Trajectory Prediction. In *CVPR*, 15251–15260.
- Kim, S.; Lee, D.; Kang, S.; Lee, S.; and Yu, H. 2023. Learning topology-specific experts for molecular property prediction. In *AAAI*, volume 37, 8291–8299.

- Kosaraju, V.; Sadeghian, A.; Martín-Martín, R.; Reid, I.; Rezatofighi, H.; and Savarese, S. 2019. Social-bigat: Multimodal trajectory forecasting using bicycle-gan and graph attention networks. *Neurips*, 32.
- Lee, S.; Lee, J.; Yu, Y.; Kim, T.; and Lee, K. 2024. Mart: Multiscale relational transformer networks for multi-agent trajectory prediction. In *ECCV*, 89–107.
- Lerner, A.; Chrysanthou, Y.; and Lischinski, D. 2007. Crowds by example. In *Computer graphics forum*, volume 26, 655–664.
- Li, R.; Katsigiannis, S.; Kim, T.-K.; and Shum, H. P. 2025a. BP-SGCN: Behavioral Pseudo-Label Informed Sparse Graph Convolution Network for Pedestrian and Heterogeneous Trajectory Prediction. *TNNLS*.
- Li, R.; Katsigiannis, S.; and Shum, H. P. 2022. Multiclass-SGCN: Sparse Graph-Based Trajectory Prediction with Agent Class Embedding. In *ICIP*, 2346–2350. IEEE.
- Li, R.; Qiao, T.; Katsigiannis, S.; Zhu, Z.; and Shum, H. P. 2025b. Unified Spatial-Temporal Edge-Enhanced Graph Networks for Pedestrian Trajectory Prediction. *TCSVT*.
- Liu, J.; Mao, X.; Fang, Y.; Zhu, D.; and Meng, M. Q.-H. 2021. A survey on deep-learning approaches for vehicle trajectory prediction in autonomous driving. In *ICRB*, 978–985.
- Lu, W.; Guan, Z.; Zhao, W.; Yang, Y.; and Jin, L. 2024. Nodemixup: Tackling under-reaching for graph neural networks. In *AAAI*, volume 38, 14175–14183.
- Luber, M.; Stork, J. A.; Tipaldi, G. D.; and Arras, K. O. 2010. People tracking with human motion predictions from social forces. In *ICRA*, 464–469.
- Luo, Y.; Cai, P.; Bera, A.; Hsu, D.; Lee, W. S.; and Manocha, D. 2018. Porca: Modeling and planning for autonomous driving among many pedestrians. *RAL*, 3(4): 3418–3425.
- Mao, W.; Xu, C.; Zhu, Q.; Chen, S.; and Wang, Y. 2023. Leapfrog Diffusion Model for Stochastic Trajectory Prediction. In *CVPR*.
- Mohamed, A.; Qian, K.; Elhoseiny, M.; and Claudel, C. 2020. Social-stgcnn: A social spatio-temporal graph convolutional neural network for human trajectory prediction. In *CVPR*, 14424–14432.
- Mu, S.; and Lin, S. 2025. A comprehensive survey of mixture-of-experts: Algorithms, theory, and applications. *Arxiv*.
- Mustafa, B.; Riquelme, C.; Puigcerver, J.; Jenatton, R.; and Houlsby, N. 2022. Multimodal contrastive learning with limoe: the language-image mixture of experts. *NeurIPS*, 35: 9564–9576.
- Pellegrini, S.; Ess, A.; Schindler, K.; and Van Gool, L. 2009. You'll never walk alone: Modeling social behavior for multitarget tracking. In *ICCV*, 261–268.
- Qian, C.; Manolache, A.; Morris, C.; and Niepert, M. 2024. Probabilistic Graph Rewiring via Virtual Nodes. In *Neurips*.
- Qiao, T.; Li, R.; Li, F. W.; Kubotani, Y.; Morishima, S.; and Shum, H. P. 2025. Geometric visual fusion graph neural networks for multi-person human-object interaction recognition in videos. *ESWA*.

- Qiao, T.; Li, R.; Li, F. W.; and Shum, H. P. 2024. From category to scenery: An end-to-end framework for multiperson human-object interaction recognition in videos. In *ICPR*, 262–277.
- Qiao, T.; Men, Q.; Li, F. W. B.; Kubotani, Y.; Morishima, S.; and Shum, H. P. H. 2022. Geometric Features Informed Multiperson Human-object Interaction Recognition in Videos. In *ECCV*.
- Riquelme, C.; Puigcerver, J.; Mustafa, B.; Neumann, M.; Jenatton, R.; Susano Pinto, A.; Keysers, D.; and Houlsby, N. 2021. Scaling vision with sparse mixture of experts. *NeurIPS*, 34: 8583–8595.
- Robicquet, A.; Sadeghian, A.; Alahi, A.; and Savarese, S. 2016. Learning social etiquette: Human trajectory understanding in crowded scenes. In *ECCV*, 549–565.
- Rusch, T. K.; Bronstein, M. M.; and Mishra, S. 2023. A survey on oversmoothing in graph neural networks. *Arxiv*.
- Shao, M.; Miao, X.; Duan, H.; Wang, Z.; Chen, J.; Huang, Y.; Wu, X.; Deng, J.; Long, Y.; and Zheng, Y. 2025a. TRACE: Temporally Reliable Anatomically-Conditioned 3D CT Generation with Enhanced Efficiency. In *International Conference on Medical Image Computing and Computer-Assisted Intervention*, 627–637. Springer.
- Shao, M.; Wang, Z.; Duan, H.; Huang, Y.; Zhai, B.; Wang, S.; Long, Y.; and Zheng, Y. 2025b. Rethinking Brain Tumor Segmentation From the Frequency Domain Perspective. *TMI*, 44(11): 4536–4553.
- Shazeer, N.; Mirhoseini, A.; Maziarz, K.; Davis, A.; Le, Q.; Hinton, G.; and Dean, J. 2017. Outrageously Large Neural Networks: The Sparsely-Gated Mixture-of-Experts Layer. In *ICLR*.
- Shi, L.; Wang, L.; Long, C.; Zhou, S.; Zhou, M.; Niu, Z.; and Hua, G. 2021. SGCN: Sparse graph convolution network for pedestrian trajectory prediction. In *CVPR*, 8994–9003.
- Veličković, P.; Cucurull, G.; Casanova, A.; Romero, A.; Lio, P.; and Bengio, Y. 2018. Graph attention networks. In *ICLR*.
- Wang, H.; Jiang, Z.; You, Y.; Han, Y.; Liu, G.; Srinivasa, J.; Kompella, R.; Wang, Z.; et al. 2023. Graph mixture of experts: Learning on large-scale graphs with explicit diversity modeling. *Neurips*, 36: 50825–50837.
- Wang, X.; Yu, F.; Dunlap, L.; Ma, Y.-A.; Wang, R.; Mirhoseini, A.; Darrell, T.; and Gonzalez, J. E. 2020. Deep mixture of experts via shallow embedding. In *UAI*, 552–562.
- Xu, C.; Li, M.; Ni, Z.; Zhang, Y.; and Chen, S. 2022a. Group-Net: Multiscale Hypergraph Neural Networks for Trajectory Prediction with Relational Reasoning. *CVPR*, 6488–6497.
- Xu, C.; Mao, W.; Zhang, W.; and Chen, S. 2022b. Remember intentions: Retrospective-memory-based trajectory prediction. In *CVPR*, 6488–6497.
- Xu, C.; Tan, R. T.; Tan, Y.; Chen, S.; Wang, Y. G.; Wang, X.; and Wang, Y. 2023. EqMotion: Equivariant Multi-Agent Motion Prediction With Invariant Interaction Reasoning. In *CVPR*.
- Xue, H.; Huynh, D. Q.; and Reynolds, M. 2018. SS-LSTM: A hierarchical LSTM model for pedestrian trajectory prediction. In *WACV*, 1186–1194.

- Yuksel, S. E.; Wilson, J. N.; and Gader, P. D. 2012. Twenty Years of Mixture of Experts. In *TNNLS*.
- Zhou, Y.; Lei, T.; Liu, H.; Du, N.; Huang, Y.; Zhao, V. Y.; Dai, A. M.; Chen, Z.; Le, Q. V.; and Laudon, J. 2022. Mixture-of-Experts with Expert Choice Routing. In *NeurIPS*.

Supplementary Material for

ViTE: Virtual Graph Trajectory Expert Router for Pedestrian Trajectory Prediction

Ruochen Li¹, Zhanxing Zhu², Tanqiu Qiao¹, Hubert P. H. Shum^{1*}

¹Department of Computer Science, Durham University, UK ²School of Electrical and Computer Science (ECS), University of Southampton, UK {ruochen.li, hubert.shum}@durham.ac.uk

This supplementary document offers additional technical and experimental details that support the findings reported in the main paper. We begin with an overview of the baseline methods used for comparison. We then describe our implementation details. Finally, we present supplementary experiments and qualitative results to further illustrate the effectiveness of our proposed framework.

Details of Baselines

- STAR (Yu et al. 2020): This model introduces a spatialtemporal graph transformer framework focusing on trajectory prediction.
- **PECNet** (Mangalam et al. 2020): This model proposes a predicted endpoint-conditioned network that captures stochastic goals and introduces a novel non-local social pooling layer for human trajectory prediction.
- GroupNet (Xu et al. 2022a): This method proposes a multiscale hypergraph neural network for multi-agent trajectory prediction.
- MemoNet (Xu et al. 2022b): MemoNet is an instancebased trajectory prediction framework that mimics human memory by retrieving similar past scenarios from a memory bank to improve prediction performance.
- MID (Gu et al. 2022): This method introduces a parameterized Markov chain and a transformer-based diffusion model for trajectory prediction
- NPSN (Bae, Park, and Jeon 2022): This method tackles trajectory variability using Quasi-Monte Carlo sampling and introduces the Non-Probability Sampling Network (NPSN) for improved prediction.
- DynGroupNet (Xu et al. 2024): This paper introduces a dynamic-group-aware model improves interaction modeling for trajectory prediction.
- **EigenTraj** (Bae, Oh, and Jeon 2023): The paper presents EigenTrajectory (EigenTraj), a method for enhancing pedestrian trajectory prediction by constructing a com
 - pact ET space to represent movement patterns.

- EqMotion (Xu et al. 2023): EqMotion predicts trajectories with Euclidean equivariance and models interactions in a transformation-invariant manner.
- LED (Mao et al. 2023): LED is a diffusion-based trajectory predictor that generates diverse outputs efficiently by using a leapfrog initializer to skip denoising steps.
- SingularTraj (Bae, Park, and Jeon 2024): The paper presents SingularTrajectory (SingularTraj), a diffusionbased framework for pedestrian trajectory prediction.
- MART (Lee et al. 2024): This paper introduces multiscale relational transformer for trajectory prediction.
- PCHGCN (Chen, Sang, and Zhao 2025): This paper introduces a high-order spatial-temporal framework for pedestrian trajectory prediction.

Implementation Details

As shown in Table 1, we summarize the key model components and training hyperparameters used in our ViTE framework. In the one-hop interaction expert, we adopt a two-layer Graph Convolutional Network (GCN) (Kipf and Welling 2017) to model local interactions. For the virtual graph module, the first stage employs a single-layer Graph Attention Network (GAT) (Veličković et al. 2018) for feature aggregation, while the second stage uses a single-layer GCN for feature distribution. We use the MultiStepLR scheduler with a decay factor of 0.5 to adjust the learning rate during training. For ETH/UCY datasets, we apply data augmentation following (Mohamed et al. 2022). The model is trained on a single NVIDIA TITAN Xp GPU for each dataset with Adam optimizer.

Supplementary Analysis

Virtual Node Mechanism Analysis

Figure 1 (left) shows the effect of virtual node count on prediction accuracy. We observe that using only one virtual node leads to suboptimal performance, likely due to limited capacity for modeling diverse global interactions. Performance improves and peaks when using three virtual nodes, indicating this configuration offers a good balance between expressiveness and efficiency. Adding more virtual nodes (e.g., four or five) results in slight degradation, suggesting that excessive

*Corresponding author

Copyright © 2026, Association for the Advancement of Artificial Intelligence (www.aaai.org). All rights reserved.

| Parameter | ЕТН | HOTEL | UNIV | ZARA1 | ZARA2 | NBA | SDD |
|------------------------|-------|--------|-------|--------|--------|--------|-------|
| Learning Rate | 0.001 | 0.0018 | 0.001 | 0.0012 | 0.0012 | 0.0005 | 0.001 |
| Training Epochs | 300 | 300 | 300 | 300 | 300 | 100 | 300 |
| Top-P Threshold | 0.5 | 0.6 | 0.5 | 0.6 | 0.5 | 0.5 | 0.5 |
| # Expert Router Layers | 3 | 3 | 3 | 3 | 3 | 2 | 1 |
| # Virtual Nodes | 3 | 3 | 3 | 3 | 3 | 2 | 1 |

Table 1: Hyperparameter settings for each dataset.

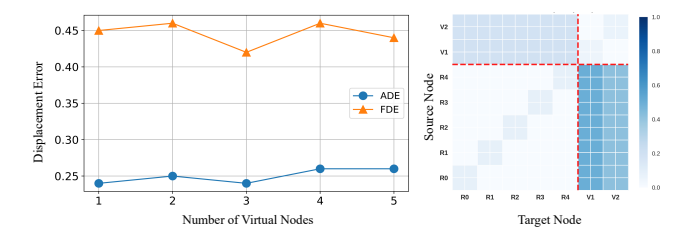


Figure 1: Analysis of virtual node mechanisms. Prediction accuracy (ADE/FDE) with varying virtual node counts on UNIV subset (**Left**). Attention map for message-passing between real nodes (R0–R4) and virtual nodes (V1–V2) (**Right**).

nodes may introduce redundant or noisy interactions that hinder learning.

To better understand how virtual nodes function, we visualize the attention weights between real nodes (R0–R4) and virtual nodes (V1–V2) in Figure 1 (right). The attention map reveals that both virtual nodes maintain strong connections with all real agents, confirming their role as global aggregators. Notably, V1 and V2 exhibit different attention patterns, indicating complementary specialization. The asymmetric structure of the map—where information flows from real nodes to virtual nodes and then back—also reflects our two-stage design, enabling virtual nodes to collect and redistribute high-level context across the graph.

More Qualitative Results

Figure 2 presents qualitative results of our framework across the five ETH/UCY subsets, arranged from left to right in order of increasing scene complexity. These scenarios exhibit diverse and stochastic pedestrian movement behaviors, including nonlinear movements, abrupt direction changes, and densely entangled trajectories. Despite such challenges, our model consistently produces accurate and socially compliant predictions that closely follow ground-truth trajectories.

In relatively simple environments such as ETH and HO-TEL, the predicted trajectories align smoothly with historical trajectories. For mid-level complexity scenes like ZARA1, where subtle group interactions and moderate scene dynamics are present, our model effectively maintains prediction accuracy while preserving socially aware movement patterns. In the more complex subsets ZARA2 and UNIV, which contain frequent agent crossings and rapid directional changes, our approach remains robust, accurately anticipating individual behaviors and inter-agent spacing. These results highlight

the strong generalization ability of our expert-driven interaction modeling across both structured and highly dynamic pedestrian scenarios.

Failure Case Discussion

While our model demonstrates strong overall performance across diverse scenes, we observe certain failure cases in highly interactive or converging pedestrian scenarios. As shown in Figure 3, when multiple agents approach a shared goal region or intersecting paths, the model may predict future trajectories that lead to potential collisions. This issue often occurs when agents have ambiguous or overlapping motion patterns during the observation period. Without explicit collision avoidance or intent modeling, the model may overfit to historical movements and fail to anticipate social negotiation. While our interaction modeling performs well in general, future work could explore collision-aware objectives or intent-aware prediction to improve physical plausibility and social compliance.

References

Bae, I.; Oh, J.; and Jeon, H.-G. 2023. Eigentrajectory: Lowrank descriptors for multi-modal trajectory forecasting. In *ICCV*, 10017–10029.

Bae, I.; Park, J.-H.; and Jeon, H.-G. 2022. Non-probability sampling network for stochastic human trajectory prediction. In *CVPR*, 6477–6487.

Bae, I.; Park, Y.-J.; and Jeon, H.-G. 2024. Singulartrajectory: Universal trajectory predictor using diffusion model. In *CVPR*, 17890–17901.

Chen, W.; Sang, H.; and Zhao, Z. 2025. PCHGCN: Physically Constrained Higher-Order Graph Convolutional Network for Pedestrian Trajectory Prediction. *IEEE Internet of Things Journal*, 12(13): 25033–25045.

Gu, T.; Chen, G.; Li, J.; Lin, C.; Rao, Y.; Zhou, J.; and Lu, J. 2022. Stochastic Trajectory Prediction via Motion Indeterminacy Diffusion. In *CVPR*.

Kipf, T. N.; and Welling, M. 2017. Semi-Supervised Classification with Graph Convolutional Networks. In *ICLR*.

Lee, S.; Lee, J.; Yu, Y.; Kim, T.; and Lee, K. 2024. Mart: Multiscale relational transformer networks for multi-agent trajectory prediction. In *ECCV*, 89–107.

Mangalam, K.; Girase, H.; Agarwal, S.; Lee, K.-H.; Adeli, E.; Malik, J.; and Gaidon, A. 2020. It is not the journey but the destination: Endpoint conditioned trajectory prediction. In *ECCV*, 759–776.

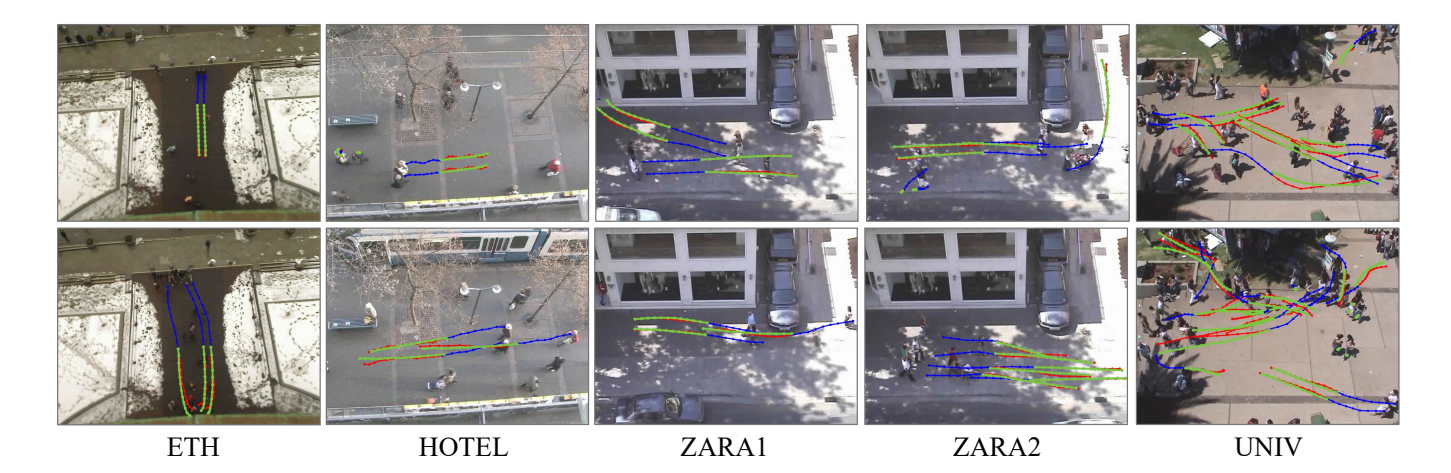


Figure 2: Qualitative results on ETH/UCY datasets. Historical trajectories are in blue, ground-truth trajectories are in red, and predicted trajectories are in green.

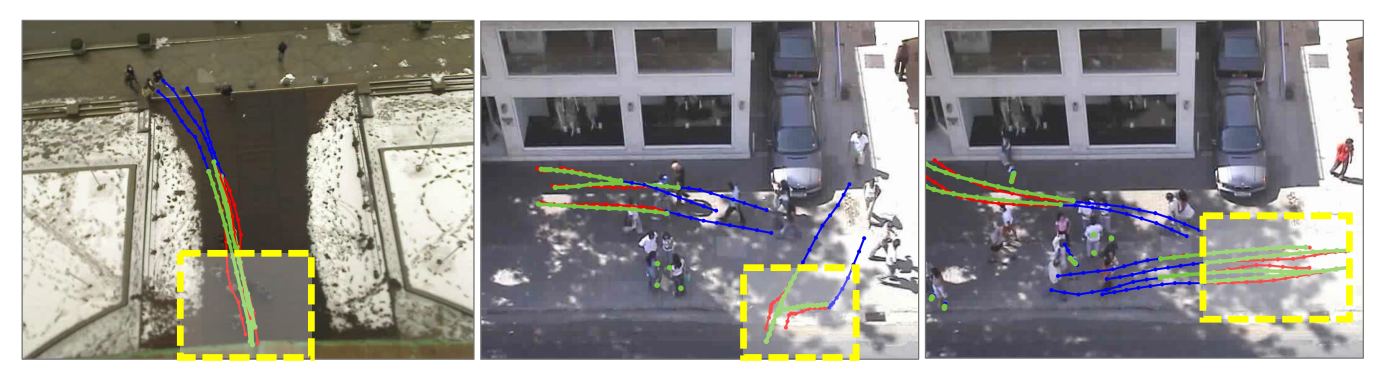


Figure 3: Illustration of a failure case. Historical trajectories are in blue, ground-truth trajectories are in red, and predicted trajectories are in green. Regions with potential trajectory overlap are highlighted by yellow boxes.

Mao, W.; Xu, C.; Zhu, Q.; Chen, S.; and Wang, Y. 2023. Leapfrog Diffusion Model for Stochastic Trajectory Prediction. In *CVPR*.

Mohamed, A.; Zhu, D.; Vu, W.; Elhoseiny, M.; and Claudel, C. 2022. Social-implicit: Rethinking trajectory prediction evaluation and the effectiveness of implicit maximum likelihood estimation. In *ECCV*, 463–479.

Veličković, P.; Cucurull, G.; Casanova, A.; Romero, A.; Lio, P.; and Bengio, Y. 2018. Graph attention networks. In *ICLR*.

Xu, C.; Li, M.; Ni, Z.; Zhang, Y.; and Chen, S. 2022a. Group-Net: Multiscale Hypergraph Neural Networks for Trajectory Prediction with Relational Reasoning. *CVPR*, 6488–6497.

Xu, C.; Mao, W.; Zhang, W.; and Chen, S. 2022b. Remember intentions: Retrospective-memory-based trajectory prediction. In *CVPR*, 6488–6497.

Xu, C.; Tan, R. T.; Tan, Y.; Chen, S.; Wang, Y. G.; Wang, X.; and Wang, Y. 2023. EqMotion: Equivariant Multi-Agent Motion Prediction With Invariant Interaction Reasoning. In *CVPR*.

Xu, C.; Wei, Y.; Tang, B.; Yin, S.; Zhang, Y.; Chen, S.; and Wang, Y. 2024. Dynamic-group-aware networks for multi-

agent trajectory prediction with relational reasoning. *Neural Networks*, 170: 564–577.

Yu, C.; Ma, X.; Ren, J.; Zhao, H.; and Yi, S. 2020. Spatio-temporal graph transformer networks for pedestrian trajectory prediction. In *ECCV*, 507–523.